Supplementary Materials: Phase diagram of palladium characterized *in situ via* synchrotron X-ray diffraction coupled with laser-heated diamond anvil cell

Simone Anzellini[1*], Samuel R. Baty[2], Leonid Burakovsky[2], Jose Luis Rodrigo-Ramon[1], Jorge Rodríguez-Lescure González[1], Pablo Botella[1], Egor Koemets[3], Daniel Errandonea[1]

[1]Department of Applied Physics - Institute of Materials Science, Matter at High Pressure (MALTA) Consolider Team, University of Valencia, C/Dr. Moliner 50, Burjassot, 46100, Valencia, Spain.
[2]Theoretical Divisions, Los Alamos National Laboratory, Los Alamos, 87545 NM, United States of America.
[3]Diamond Light Source Ltd., Harwell Science and Innovation Campus, Diamond House, Didcot, OX11 0DE, Oxfordshire, UK.

*Corresponding author(s). E-mail(s): simone2.anzellini@uv.es;

Abstract

Transition metals exhibit complex structural behavior under extreme conditions, yet their high-pressure–high-temperature phase diagrams remain poorly constrained experimentally. Palladium exemplifies this problem, with a predicted face-centered cubic (***fcc***) to body-centered cubic (***bcc***) transition that has eluded experimental detection. Here we demonstrate that this discrepancy arises from kinetic constraints and can be overcome through melt-mediated pathways. Using *in situ* synchrotron X-ray diffraction in a laser-heated diamond anvil cell, we map the phase diagram of palladium up to 107 GPa and 6800 K and directly access a ***bcc*** polymorph *via* rapid quenching from the liquid. We show that, although thermodynamically competitive, the ***bcc*** phase is kinetically inaccessible along the solid-state pathway, but becomes stabilized near melting where enhanced atomic mobility enables structural selection. This establishes a general mechanism by which high-pressure phases can remain hidden in experiments despite theoretical stability. Our results reconcile long-standing theory–experiment inconsistencies

for palladium and suggest that similar kinetic limitations may govern phase stability across ***d***-band metals. In addition, we determine a high-precision melting curve and thermal equation of state in quantitative agreement with *ab initio* simulations, providing a benchmark for materials under extreme conditions. These findings redefine the experimental accessibility of high-pressure phases and call for a reassessment of phase diagrams where kinetic effects have been overlooked.

Keywords: Melting, Extreme Conditions, Transition Metals, Laser-heating

Supplementary Information

The LH-DAC experiment was performed using the LH-system built at the extreme conditions beamline I15 of Diamond Light Source. A detailed description of the system can be found in Anzellini *et al.*[1]. However, in Supplementary Fig. 1 we are reporting the schematics of the adopted system for reference. Supplementary Figure 2 illustrates

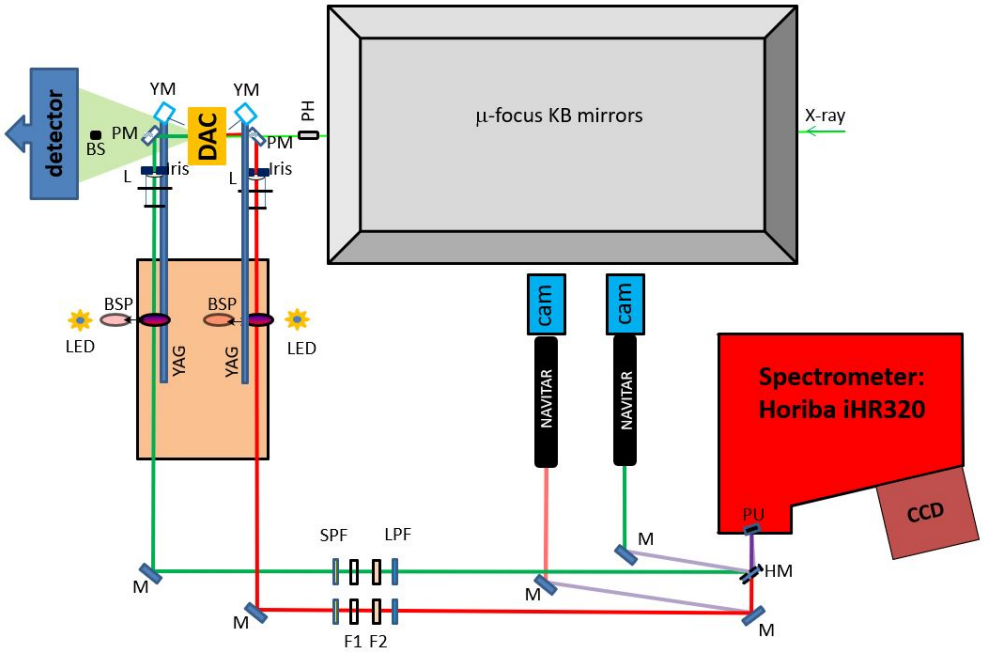

Supplementary Figure 1 Schematics of the laser-heating system used on the I15 beamline: Red and green lines represent the down and up-stream optical paths, respectively. The various components abbreviations are as follows: BS: beam-stop; L: lens; YM: YAG mirror; PH: pinhole; PM: Perforated mirror; BSP: Removable beam-splitter for LED illumination of the sample; M: mirror; SPF: Short-pass filter; LPF: Long-pass filter; F1 and F2: Neutral density filters; HM: Half mirror; PU: perforated mirror at the entrance of the spectrometer.

the observed splitting of the Pd diffraction peaks in one of the experimental loadings. The depicted Pawley refinement demonstrates an excellent fit to the data, yielding lattice parameters of $a = 3.890$ Å for pure Pd and $a = 3.980$ Å for an expanded fcc phase. This figure also provides a comparison between the current dataset and the results reported by Fedotenko *et al.* [2] regarding the characterization of PdC in LH-DAC experiments.The strong agreement between our observations and the reported values for PdC suggests that palladium carbide formed during the sample preparation stage. Notably, these peaks were present from the initial pressure increase, despite no laser heating having been applied to this specific sample. A critical difference in the preparation of this loading was the pre-heating of the Pd powder in an oven at 250°C. It is hypothesized that the Pd reacted with carbon from the diamond anvils—which had been previously degraded during prior laser-heating sessions—during the mechanical foil preparation as the powder was pressed between the anvils. Supplementary Figure

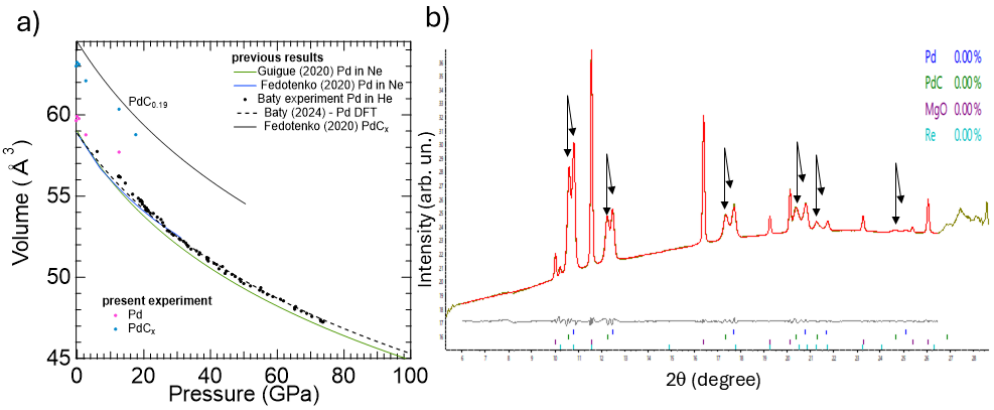

Supplementary Figure 2 Chemical reaction: (a) EoS of pure Pd and PdC as reported by previous studies [2–4], compared with data PdC data obtained in the present experiment. (b) Pawley refinement showing the presence of the Pd peak splitting due to the formation of PdC_x.

3 presents the Pawley refinements of a diffraction pattern collected *in situ* at 72 GPa and 4478 K, where palladium remains exclusively in the fcc phase. This is compared to XRD data acquired immediately following a thermal quench. Upon quenching, the appearance of new diffraction peaks is observed; these features are well-indexed by a bcc phase with a molar volume nearly identical to that of the fcc phase. The calculated volume difference is approximately 0.4%, suggesting a volume-conservative $fcc \rightarrow bcc$ phase transition, consistent with previous theoretical predictions [3, 5, 6].

Theoretical simulations

The theoretical investigation of the thermal EoS for palladium was conducted using the Vienna Ab initio Simulation Package (VASP). The electronic structure was modeled using a $[^{30}\mathrm{Zn}]\, 4p^6 4d^{10}$ core-valence configuration, assigning 16 outermost electrons to

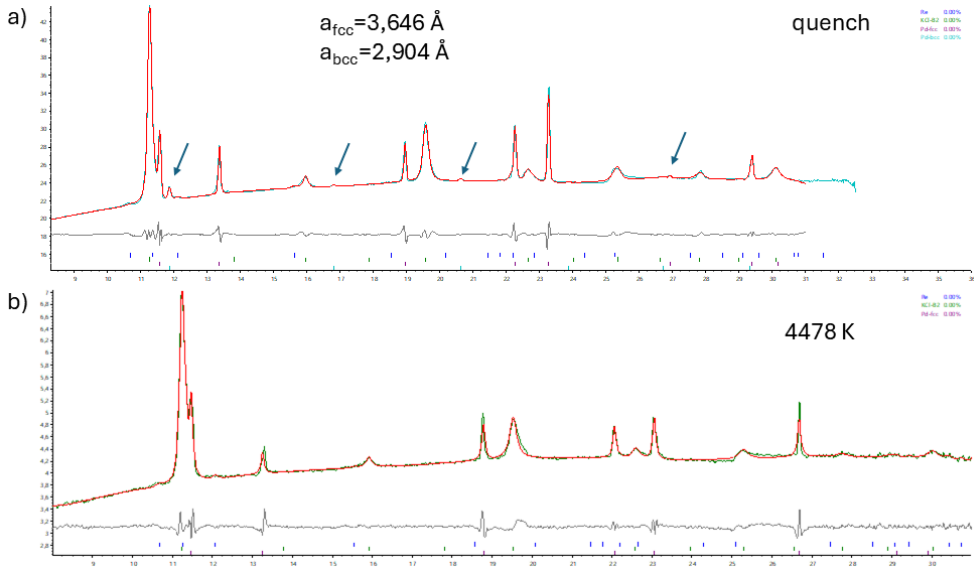

Supplementary Figure 3 New solid phase: Pawley refinements of XRD patterns collected at approximately 72 GPa. The pattern obtained at 4478 K (b) exhibits a pure *fcc* phase, while the subsequent thermal quench (a) reveals the emergence of new diffraction peaks. These features are well-indexed by a *bcc*-Pd structure that maintains a molar volume nearly identical to the parent *fcc* phase, consistent with a volume-conservative phase transition.

the valence shell. Valence electrons were expanded in a plane-wave basis set with a kinetic energy cutoff of 350 eV, while core-electron interactions were described by the projector augmented-wave (PAW) method. Various exchange-correlation functionals (XCF) within the density functional theory (DFT) framework—including local density (LDA) and generalized gradient approximations (GGA) such as PBE, PBEsol, and AM05—were evaluated. Previous studies [7–9] established that PBEsol and AM05 provide superior accuracy for Pd, particularly regarding the ambient lattice constant and isothermal bulk modulus. Consequently, we calculated the thermal EOS of *fcc*-Pd using a broad suite of functionals, including LDA, PBE, PBEsol, AM05, PW91, revPBE, and RPBE. The thermal EOS is formulated as a function of density (ρ) and temperature (T):

$$P(\rho, T) = P(\rho, 0) + CT + DT^2$$

where $P(\rho, 0)$ represents the cold curve ($T = 0$ K), and C and D are material-specific constants. Typically, $C = \alpha B_T$, where α is the thermal expansion coefficient and K_T is the isothermal bulk modulus; their product is assumed to be temperature-independent, while D accounts for higher-order thermal corrections. The cold curve $P(\rho, 0)$ was modeled using a third-order Birch-Murnaghan EoS:

$$P(\rho, 0) = \frac{3}{2} K_0 \left(\eta^{7/3} - \eta^{5/3}\right) \left[1 + \frac{3}{4}(K_0' - 4)\left(\eta^{2/3} - 1\right)\right]$$

Here, $\eta = \rho/\rho_0$, and the subscript 0 denotes properties at $T = 0$ K and $P = 0$ GPa. For fcc-Pd using the AM05 functional, the resulting parameters are $\rho_0 = 12.175$ g/cm^3, $K_0 = 197.3$ GPa, and $K_0' = 5.3$. These values align closely with previous PBEsol results [3] ($\rho_0 = 12.09$, $K_0 = 195.9 \pm 2.5$ GPa, $K_0' = 5.1 \pm 0.1$) and are consistent with reported experimental values ($K_0 = 192 \pm 8$ GPa and $K_0' = 4.7 \pm 4$). Notably, the calculated ρ_0 and K_0 deviate from experimental benchmarks by less than 0.7% and 1%, respectively [7, 9].

Finite-temperature simulations were performed *via* quantum molecular dynamics (QMD) using the Nosé thermostat algorithm. Calculations used a 32-atom ($2 \times 2 \times 2$) supercell with a dense $15 \times 15 \times 15$ k-point mesh. Rigorous convergence tests were conducted to ensure the stability of the results with respect to mesh density and energy cutoffs. For each XCF implementation, 60 QMD runs were executed at fixed temperatures ranging from 500 K to 5000 K (in 500 K increments) across six distinct lattice constants, corresponding to a pressure range of 0–250 GPa. Each simulation consisted of 15,000 time steps with a 1 fs duration, totaling 15 ps per trajectory to ensure adequate equilibration and statistical sampling.

Direct comparison with experimental data reveals that the AM05 functional provides the most accurate description of the thermal EoS for Pd over the entire 0–250 GPa range. The PBEsol functional yields results nearly identical to AM05 and is considered equally reliable for this system. Detailed numerical results for the AM05-based thermal EoS, including cold curve values and finite-temperature data, are provided in Supplementary Table 1.

T	a	P	a	P	a	P	a	P	a	P	a	P
0	4.00	-15.05	3.85	3.466	3.70	39.70	3.55	104.9	3.45	174.6	3.40	221.3
500	4.00	-14.73	3.85	5.070	3.70	41.70	3.55	106.1	3.45	177.5	3.40	222.4
1000	4.00	-12.58	3.85	7.137	3.70	43.81	3.55	107.8	3.45	179.9	3.40	223.9
1500	4.00	-9.247	3.85	9.506	3.70	45.97	3.55	110.0	3.45	182.0	3.40	225.8
2000	4.00	-5.389	3.85	12.02	3.70	48.14	3.55	112.5	3.45	183.7	3.40	228.1
2500	4.00	-1.650	3.85	14.52	3.70	50.25	3.55	115.1	3.45	185.0	3.40	230.7
3000	4.10	-8.553	3.95	2.093	3.80	24.73	3.65	66.50	3.50	150.1	3.40	233.6
3500	4.10	-6.511	3.95	5.436	3.80	27.53	3.65	73.71	3.50	153.0	3.40	237.1
4000	4.15	-7.657	4.00	2.368	3.85	20.35	3.70	55.68	3.55	122.1	3.40	239.7
4500	4.15	-5.109	4.00	4.196	3.85	23.40	3.70	58.28	3.55	123.6	3.40	241.9
5000	4.20	-2.432	4.00	9.194	3.80	36.54	3.60	101.2	3.50	160.6	3.40	244.4

Supplementary Table 1 Theoretical results: The 66 *ab initio* data points for the thermal EoS of fcc-Pd obtained using the AM05 implementation of GGA. Temperature, lattice parameter and pressure are expressed in K, $\AA$ and GPa, respectively.

Alternative DFT implementations consistently yield P values higher than those derived from AM05, resulting in greater deviations from experimental benchmarks. For example, at a lattice constant of $a = 3.2$ Å, the calculated cold pressures are 510.7 GPa (AM05), 519.3 GPa (PBEsol), and 542.8 GPa (PBE). These relative differences persist at finite temperatures. Among the available LDA functionals, the LDA-CA (or -PZ) implementation—using the Pd_pv_ pseudopotential in VASP—demonstrates the highest performance. In the high-density regime, LDA-CA yields pressure values

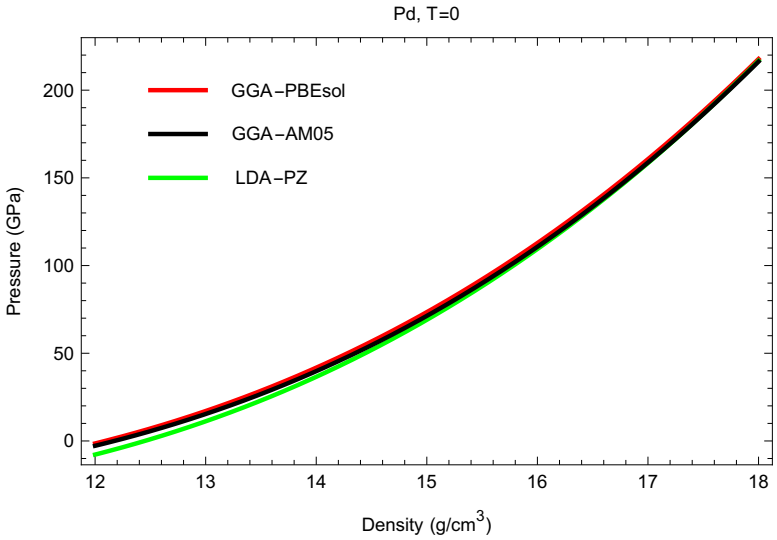

Supplementary Figure 4 Comparison of cold EoS produced by three different implementations of DFT: PBEsol and AM05 for GGA, and LDA-CA for LDA.

that converge closely with experimental data; for instance, at the aforementioned lattice constant, it predicts 508.4 GPa, a value virtually indistinguishable from the AM05 result. However, LDA-CA exhibits limitations at lower pressures, where it overestimates densities (underestimates volumes) compared to GGA functionals. This leads to lower pressure values than either PBEsol or AM05 at identical ρ and T. Specifically, at the AM05 equilibrium density (ρ_0 = 12.175 g/cm^3, a = 3.872 Å), where $P = 0$ GPa, LDA-CA predicts a pressure of -4.7 GPa. As pressure increases, the thermal EoS produced by LDA-CA approaches that of AM05. Above approximately 100 GPa, the pressures calculated by AM05, PBEsol, and LDA-CA become nearly identical, as demonstrated by the direct comparison in Supplementary Figure 4. The best fit of the thermal EOS model described by Eqs. (1) and (2) to the 60 finite-temperature data points yields the coefficients $C = 5.6 \times 10^{-3}$ GPa/K and $D = -2.0 \times 10^{-7}$ GPa/K^2. This model reproduces the calculated pressures within a margin of 1–2 GPa. Neglecting the second-order term (D) results in $C = 4.8 \times 10^{-3}$ GPa/K, which maintains an accuracy of 2–3 GPa. This simplified coefficient is consistent with the experimental product of the ambient thermal expansion coefficient (α_0) and the isothermal bulk modulus, which is $3.5(2) \times 10^{-3}$ GPa/K. The 27% discrepancy likely arises from the assumption of a temperature-independent αK_T product when fitting QMD results across the extensive 0–5000 K range.The reliability of the derived thermal EoS was further validated by calculating the density of fcc-Pd at the ambient melting point (T_m = 1828 K). Solving $P(\rho, 1828) = 0$ yields a density of ρ = 11.509 g/cm^3, which is within 3% of the experimental value of 11.179 g/cm^3 [**?**]. The stability and temporal evolution of temperature and pressure during the QMD simulations are illustrated in Supplementary Figures 5 and 6. These figures represent a specific run at a = 3.4 Å with a target temperature of 3500 K, which resulted in an equilibrium pressure of

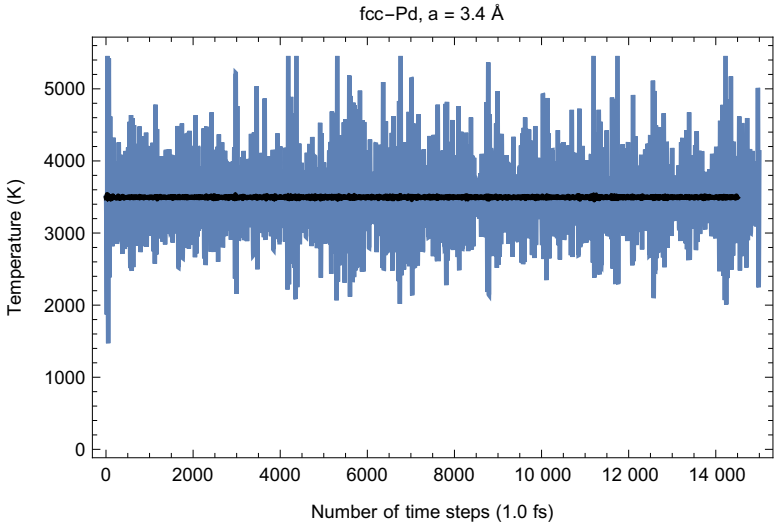

Supplementary Figure 5 The time evolution of T in a QMD run of fcc-Pd with a unit cell of 3.4 Å and with average T fixed at 3500 K using the AM05 implementation of DFT. Shown as a black line is the running average.

237.1 GPa. The use of the Nosé algorithm ensures controlled oscillations around the target equilibrium values, as evidenced by the running averages.

In conclusion, while LDA-CA performs exceptionally well at high compression, the GGA functionals (AM05 and PBEsol) offer a more consistent treatment across the entire pressure range, particularly near ambient conditions. The excellent agreement between the derived model and experimental density at the melting point confirms the robustness of the computational approach for modeling Pd under extreme thermodynamic conditions.

Experimental data

All the information obtained from the data collected from the solid (fcc) Pd during the LH-DAC experiments are reported in Supplementary Tables 2, 3 and 4. In particular, we are reporting the extracted lattice parameters of Pd and the used PTM (KCl), the T measured from spectral-radiometry from both sides of the sample and the corresponding thermal P measured from the thermal EoS of Dewaele *et al.*[10]

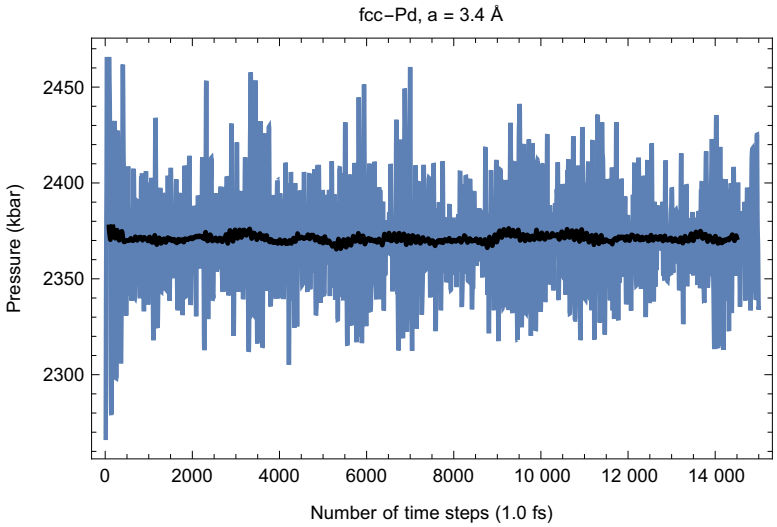

Supplementary Figure 6 The same as in Supplementary Fig. 5 for the time evolution of P.

Run	aKCl (Å)	aPd (Å)	P (GPa)	TUS (K)	TDS (K)	phase
J5	3.242	3.751	29.6(1)	300	300	solid
	3.242	3.756	32(2)	1570(210)	1769(234)	solid
	3.243	3.758	32(2)	1554(249)	1756(215)	solid
	3.245	3.765	32(2)	1592(185)	1756(223)	solid
	3.245	3.765	33(2)	1616(244)	2210(356)	solid
	3.245	3.766	33(2)	1754(301)	2420(313)	solid
	3.245	3.768	34(3)	1760(291)	2535(265)	solid
	3.244	3.773	34(3)	1805(345)	2526(238)	solid
	3.245	3.775	34(2)	1759(229)	2475(181)	solid
	3.248	3.774	34(3)	1866(219)	2886(221)	solid
	3.246	3.768	34(3)	1865(203)	2564(225)	solid
	3.246	3.766	35(3)	2115(253)	3267(457)	solid
	3.246	3.781	35(3)	1980(229)	2943(372)	solid
	3.247	3.777	34(3)	1973(213)	2628(300)	solid
	3.245	3.775	36(4)	2247(258)	3551(591)	liquid
	3.246	3.770	39(5)	3063(271)	4718(757)	liquid
	3.248	3.783	38(5)	2856(222)	4413(715)	liquid
S-g2-4	3.152	3.713	47(2)	1646(201)	1934(238)	solid
	3.152	3.710	47(2)	1620(210)	1961(252)	solid
	3.152	3.716	47(2)	1642(236)	2227(325)	solid
	3.152	3.717	47(2)	1650(243)	2332(340)	solid
	3.152	3.713	48(3)	1692(269)	2489(455)	solid
	3.152	3.713	48(3)	1703(298)	2577(350)	solid
	3.152	3.717	49(3)	1791(138)	2940(361)	solid
	3.154	3.715	48(3)	1777(140)	2883(353)	solid
	3.153	3.715	49(3)	1794(105)	3047(292)	solid
	3.153	3.717	49(3)	1804(123)	3158(434)	solid
	3.153	3.717	50(3)	1976(85)	3370(310)	solid
	3.153	3.722	50(4)	1939(78)	3445(379)	solid
	3.153	3.721	50(4)	2097(126)	3585(185)	solid
	3.153	3.723	50(4)	2101(82)	3636(169)	solid
	3.153	3.721	51(4)	2154(114)	3905(144)	solid
	3.154	3.717	51(4)	2166(103)	4064(192)	liquid
J1-g2-2	3.126622	3.6827919	48.1(1)	300	300	solid
	3.128526	3.6873679	51(2)	1765(328)	2117(562)	solid
	3.1275699	3.6914849	51(2)	1433(273)	1734(444)	solid
	3.1249051	3.6920099	51(2)	1389(297)	1763(614)	solid
	3.1248529	3.7025881	51(2)	1427(416)	1798(848)	solid
	3.1248181	3.6947501	52(2)	1648(257)	2148(337)	solid
	3.1250861	3.6980901	52(2)	1748(302)	2332(337)	solid
	3.1253569	3.699126	53(3)	1813(302)	2593(363)	solid
	3.1253779	3.7065239	53(3)	1973(275)	2791(391)	solid
	3.1253221	3.712868	54(3)	2011(283)	3017(315)	solid
	3.1253309	3.713542	54(3)	2126(287)	3099(285)	solid
	3.125859	3.7090061	55(4)	2257(305)	3454(348)	solid
	3.1254959	3.708571	55(4)	2305(289)	3550(326)	solid
	3.125772	3.70451	55(4)	2350(306)	3732(363)	solid
	3.1261001	3.7064021	55(4)	2370(336)	3760(312)	solid
	3.1261971	3.707283	56(4)	2516(353)	3988(352)	liquid

Supplementary Table 2 Experimental results: Table containing all the quantities measured during the LH-DAC experiment. In particular, aKCl and aPd represent the lattice parameters of KCl and Pd, respectively. P is the pressure determined from the thermal EoS of Dewaele *et al.*[10] for KCl. TUS and TDS represent the T measured by spectral-radiometry from the up-stream (US) and the downstream (DS) side of the sample, respectively. The error in the determined P and T is represented in the parentesis of each measurement, while for the lattice parameters we have evaluated an error of the order of 0.002 Å that agrees with the typical resolution associated with synchrotron XRD measurements.

Run	aKCl (Å)	aPd (Å)	P (GPa)	TUS (K)	TDS (K)	phase
J1-g2-3	3.100	3.669	53.5(1)	300	300	solid
	3.102	3.686	57(2)	1724(281)	2118(276)	solid
	3.096	3.670	61(4)	2148(117)	3619(426)	solid
	3.103	3.689	61(4)	2348(173)	4069(477)	solid
	3.104	3.690	61(4)	2443(251)	4150(518)	solid
	3.104	3.692	61(5)	2729(103)	4427(475)	solid
	3.105	3.700	61(5)	2791(104)	4446(479)	solid
	3.106	3.702	62(5)	2902(106)	4847(585)	liquid
	3.106	3.702	62(5)	2870(102)	4748(535)	liquid
S2-1	3.043	3.638	71(2)	1742(408)	2125(252)	solid
	3.043	3.639	71(2)	1726(264)	2105(356)	solid
	3.043	3.639	71(2)	1746(246)	2128(308)	solid
	3.044	3.640	71(2)	1803(237)	2131(291)	solid
	3.044	3.641	71(2)	1680(250)	2109(272)	solid
	3.043	3.638	71(2)	1752(266)	2142(297)	solid
	3.045	3.643	70(2)	1527(194)	2031(286)	solid
	3.044	3.641	70(2)	1489(160)	2000(278)	solid
	3.045	3.642	70(2)	1492(181)	2018(308)	solid
	3.045	3.645	71(2)	1933(241)	2440(286)	solid
	3.045	3.647	72(3)	2048(258)	2667(395)	solid
	3.046	3.650	72(3)	2100(256)	2782(461)	solid
	3.045	3.650	72(3)	2152(277)	2817(433)	solid
	3.046	3.652	71(2)	2365(307)	2312(600)	solid
	3.046	3.654	73(3)	2401(311)	3253(824)	solid
	3.046	3.653	74(4)	2591(449)	3729(718)	solid
	3.046	3.672	78(6)	2508(306)	5652(355)	liquid
	3.050	3.672	70(3)	2349(407)	2637(670)	solid
	3.051	3.650	70(3)	2372(449)	2619(405)	solid
J2-1	3.022	3.626	77(2)	1619(341)	2154(366)	solid
	3.022	3.627	78(3)	1742(191)	2748(413)	solid
	3.023	3.628	79(3)	2034(237)	3357(331)	solid
	3.024	3.629	80(4)	2121(249)	3721(313)	solid
	3.025	3.629	81(5)	2306(353)	4382(394)	solid
	3.024	3.633	81(5)	2422(399)	4573(652)	solid
	3.025	3.633	81(5)	2425(313)	4504(781)	solid
	3.025	3.635	82(5)	2564(453)	5011(484)	solid
	3.025	3.633	83(6)	2712(300)	5458(542)	liquid
	3.024	3.641	85(6)	2862(300)	6006(731)	liquid
	3.026	3.634	84(6)	3001(500)	6002(750)	liquid
J2-2	2.989	3.607	83.0(1)	300	300	solid
	2.990	3.609	86(2)	1646(381)	2126(513)	solid
	2.989	3.609	86(2)	1556(294)	2016(414)	solid
	2.989	3.609	86(2)	1516(238)	1982(407)	solid
	2.989	3.610	86(2)	1514(203)	2079(386)	solid

Supplementary Table 3 Experimental results: Table containing all the quantities measured during the LH-DAC experiment. In particular, aKCl and aPd represent the lattice parameters of KCl and Pd, respectively. P is the pressure determined from the thermal EoS of Dewaele *et al.*[10] for KCl. TUS and TDS represent the T measured by spectral-radiometry from the up-stream (US) and the downstream (DS) side of the sample, respectively. The error in the determined P and T is represented in the parentesis of each measurement, while for the lattice parameters we have evaluated an error of the order of 0.002 Å that agrees with the typical resolution associated with synchrotron XRD measurements.

Run	aKCl (Å)	aPd (Å)	P (GPa)	TUS (K)	TDS (K)	phase
J2-2	2.989	3.610	87(2)	1606(243)	2229(419)	solid
	2.989	3.611	87(2)	1685(259)	2377(464)	solid
	2.989	3.611	88(3)	1795(257)	2583(445)	solid
	2.990	3.611	88(3)	1930(236)	2780(265)	solid
	2.990	3.614	89(3)	2048(285)	3177(240)	solid
	2.990	3.612	90(4)	2149(412)	3840(239)	solid
	2.991	3.611	91(4)	2217(271)	4134(210)	solid
	2.991	3.612	90(4)	2302(375)	4210(189)	solid
	2.993	3.614	91(5)	2393(583)	4587(200)	solid
	2.994	3.615	91(5)	2500(872)	4759(192)	liquid
	2.995	3.618	91(5)	2557(476)	5123(211)	liquid
	2.994	3.614	93(6)	2698(529)	5542(342)	liquid
	2.993	3.616	93(6)	2786(453)	5727(112)	liquid
	2.996	3.622	93(6)	2934(336)	6058(173)	liquid
S2-2	2.975	3.587	91(2)	1705(230)	2391(279)	solid
	2.974	3.587	92(2)	1761(184)	2543(170)	solid
	2.970	3.583	89.1(1)	300	300	solid
	2.971	3.588	93(2)	1790(206)	2657(197)	solid
	2.971	3.589	93(2)	1862(195)	2900(153)	solid
	2.966	3.592	96(3)	2085(214)	3673(198)	solid
	2.962	3.594	98(3)	2279(258)	4519(259)	solid
	2.965	3.596	98(4)	2470(313)	5273(333)	solid
	2.962	3.596	99(4)	2536(286)	4840(395)	solid
	2.962	3.596	99(4)	2589(286)	4971(423)	solid
	2.963	3.598	99(4)	2619(294)	5218(452)	solid
	2.962	3.597	100(4)	2710(315)	5581(478)	solid
	2.960	3.599	102(5)	2792(328)	5962(521)	liquid
S2-3	2.953	3.584	95.1(1)	300	300	solid
	2.957	3.597	103(5)	3122(240)	4524(513)	solid
	2.956	3.597	104(5)	3372(303)	5030(571)	solid
	2.952	3.598	106(6)	3538(326)	5373(492)	solid
	2.956	3.598	105(6)	3572(314)	5566(561)	solid
	2.958	3.600	105(6)	3650(317)	5559(681)	liquid
	2.952	3.596	106(6)	3499(287)	5287(552)	liquid
	2.953	3.599	106(6)	3594(303)	5417(565)	liquid
	2.960	3.599	105(6)	3912(335)	6086(568)	liquid

Supplementary Table 4 Experimental results: Table containing all the quantities measured during the LH-DAC experiment. In particular, aKCl and aPd represent the lattice parameters of KCl and Pd, respectively. P is the pressure determined from the thermal EoS of Dewaele *et al.*[10] for KCl. TUS and TDS represent the T measured by spectral-radiometry from the up-stream (US) and the downstream (DS) side of the sample, respectively. The error in the determined P and T is represented in the parentesis of each measurement, while for the lattice parameters we have evaluated an error of the order of 0.002 Å that agrees with the typical resolution associated with synchrotron XRD measurements.

References

[1] Anzellini, S. *et al.* Laser-heating system for high-pressure X-ray diffraction at the extreme condition beamline I15 at Diamond Light Source. *Journal of Synchrotron Radiation* **25** (2018).

[2] Fedotenko, T. *et al.* Synthesis of palladium carbides and palladium hydride in laser heateddiamond anvil cells. *Journal of Alloys and Compounds* **844**, 156179 (2020).

[3] Baty, S. R., Burakovsky, L., Luscher, D., Anzellini, S. & Errandonea, D. Palladium at high pressure and high temperature:a combined experimental and theoretical study. *Journal of Applied Physics* **135**, 075103 (2024).

[4] Guigue, B., Geneste, G., Leridon, B. & Loubeyre, P. An x-ray study of palladium hydridesup to 100 gpa: Synthesis and isotopic effects. *Journal of Applied Physics* **127**, 075901 (2020).

[5] Liu, Z.-L., Yang, J.-H., Cai, L.-C., Jing, F.-Q. & Alfé, D. Structural and thermodynamic properties of compressed palladium: Ab initio and moleculardynamics study. *Physical Review B* **83**, 144113 (2011).

[6] Smirnov, N. Ab initio calculations of structural stability, thermodynamic and elastic properties of Ni, Pd, Rh, and Ir at high pressures. *Journal of Applied Physics* **14**, 025901 (2023).

[7] Mattsson, A. *et al.* The AM05 density functional applied to solids. *J. Chem. Phys.* **128**, 084714 (2008).

[8] Ropo, M., Kokko, K. & Vitos, L. Assessing the Perdew-Burke-Ernzerhof exchange-correlation density functional revised for metallic bulk and surface systems. *Physical Review B* **77**, 195445 (2008).

[9] Liu, H. *et al.* Assessing r2SCAN meta-GGA functional for structural parameters, cohesive energy, mechanical modulus, and thermophysical properties of 3d, 4d, and 5d transition metals. *The Journal of Chemical Physics* **160**, 024102 (2024).

[10] Dewaele, A. *et al.* High-pressure-high-temperature equation of state of KCl and KBr. *Physical Review B - Condensed Matter and Materials Physics* **85**, 1–7 (2012).